# Direct Evidence for a Similar Molecular Mechanism Underlying Shaker Kv Channel Fast Inactivation and Clustering

**Limor Lewin†, Valerie Nirenberg†, Rinat Yehezkel, Shany Naim, Uri Abdu, Irit Orr and Ofer Yifrach**

***Department of Life Sciences and the Zlotowski Center for Neuroscience,*** *Ben-Gurion University of the Negev, POB 653, Beer Sheva 84105, Israel*

***Correspondence to Ofer Yifrach:*** *ofery@bgu.ac.il*
https://doi.org/10.1016/j.jmb.2018.12.002
***Edited by Daniel L. Minor***

## Abstract

The fast inactivation and clustering functions of voltage-dependent potassium channels play fundamental roles in electrical signaling. Recent evidence suggests that both these distinct channel functions rely on intrinsically disordered N- and C-terminal cytoplasmic segments that function as entropic clocks to time channel inactivation or scaffold protein-mediated clustering, both relying on what can be described as a "ball and chain" binding mechanism. Although the mechanisms employed in each case are seemingly analogous, both were put forward based on bulky chain deletions and further exhibit differences in reaction order. These considerations raised the question of whether the molecular mechanisms underlying Kv channel fast inactivation and clustering are indeed analogous. By taking a "chain"-level chimeric channel approach involving long and short spliced inactivation or clustering "chain" variants of the Shaker Kv channel, we demonstrate the ability of native inactivation and clustering "chains" to substitute for each other in a length-dependent manner, as predicted by the "ball and chain" mechanism. Our results thus provide direct evidence arguing that the two completely unrelated Shaker Kv channel processes of fast inactivation and clustering indeed occur according to a similar molecular mechanism.



Voltage-activated potassium channels (Kv) are membrane proteins that play a fundamental role in action potential generation, propagation, and transmission [1]. These processes rely on channel activation and inactivation gating transitions [1,2], as well as on the clustering of many ion channel molecules at unique membrane sites [3,4], including nodes of Ranvier along the neuron axon or at the post-synaptic density (PSD) [5]. While channel gating transitions determine the kinetics of potassium current flow across the membrane, the clustering process determines channel density. Changes in either ionic current shape or density, reflecting changes in the temporal and spatial dimensions, respectively, affect action potential shape and frequency [6–9] and may lead a neuron to switch to a different firing mode [10]. Defining the molecular mechanisms underlying the channel gating and clustering processes is thus important for cellular-level understanding of electrical signaling and its physiological significance.

While the mechanisms underlying activation and fast inactivation gating of the prototypical *Shaker* Kv channel are solid and long-known [11–17], the molecular mechanism underlying Kv channel clustering is only now becoming clear [18–20]. We recently suggested that *Shaker* Kv channel clustering involves a "ball and chain" mechanism, analogous to the mechanism describing the fast (N-type) channel inactivation process (Fig. 1a) [20]. According to this model, the Kv channel C-terminal tail encodes a random "chain" bearing a conserved 6-amino-acid PDZ-binding motif (the "ball") at its tip that recruits its PSD-95 scaffold protein partner (the 95 kD post-synaptic density protein). The long unstructured chain of the Kv channel serves to lead the "ball" motif to its receptor binding site found in the PDZ domains of the PSD-95 protein (Fig. 1a, upper panel), with such interaction leading to channel clustering [4,5,20]. This description is reminiscent of the classical "ball and chain" mechanism put forward by Aldrich and

colleagues in the 1990s to account for Kv channel fast inactivation (Fig. 1a, lower panel) [14,15]. Here, the random walk motion of the N-terminal inactivation "chain" allows the terminal inactivation "ball" to reach through the open activation gate of the channel and bind to its receptor site along the pore ion conduction pathway [16,17], thereby blocking the flow of potassium current through the channel.

At the heart of the proposed analogy between both Kv channel "ball and chain" mechanisms lies the observation that the rate constant for a "ball"–receptor association is "chain" length dependent. Theoretic considerations, based on a random flight model of the "ball" to its receptor site, predict power law behavior for such dependence, with a characteristic power law value of 3/2 [21]. In the case of channel clustering, systematic deletions in the Kv channel C-terminal "chain" indeed affected the kinetics of association with PSD-95 in a length-dependent manner, as predicted [20]. These results mirror earlier evidence showing that systematic deletions within the N-terminal "chain" affected the rate constant of channel entry into the inactivated state [14,15], an observation later demonstrated to adhere to the power law dependence, as expected [21]. In terms of the functional classification of intrinsically disordered proteins proposed by Dunker and colleagues [22,23], both the N- and C-terminal channel tails thus encode entropic clocks that respectively time the fast inactivation and clustering functions of the *Shaker* Kv channel [24,25]. According to this

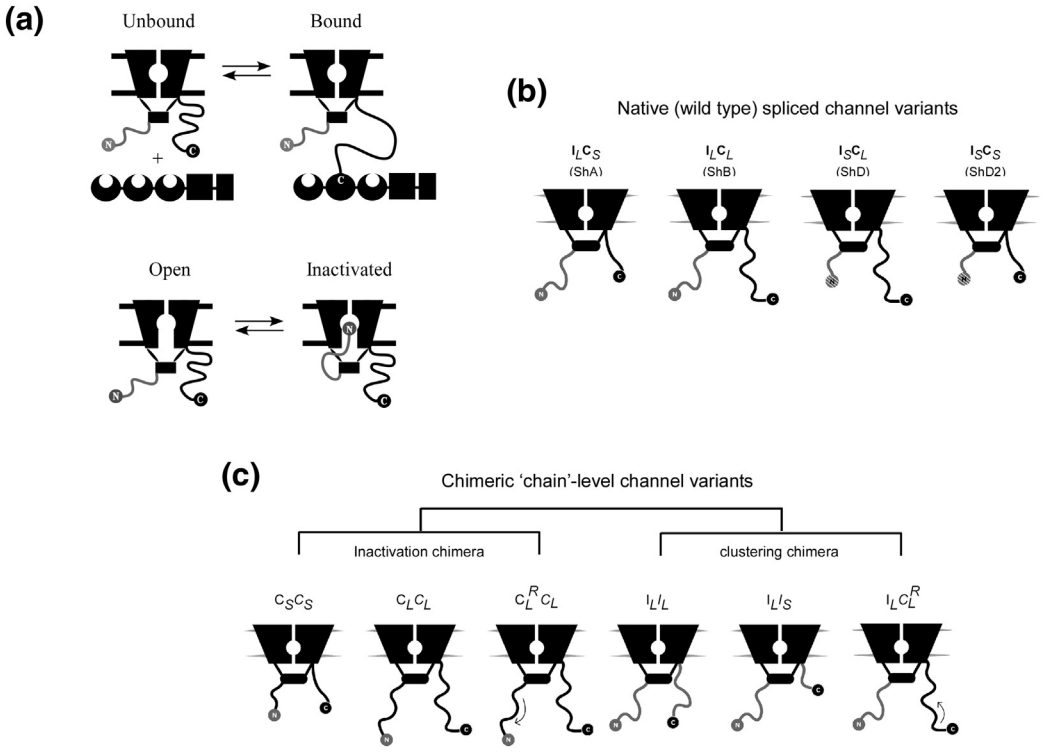


**Fig. 1.** "Chain"-level chimeric channel strategy used for analyzing the analogy between Kv channel fast inactivation and clustering mechanisms. (a) Schematic representations of the analogous "ball and chain" mechanisms that describe Kv channel inactivation and clustering (lower and upper panels, respectively). (b) The four wild-type Kv channel spliced variants used in the current study share an identical core T1 (rectangular shape) and membrane-spanning regions (voltage-sensing and pore domains) but different N- and C-terminal ends. The variants represent the four possible combinations of channels containing either long (L) or short (S) inactivation (I) and clustering (C) "chains" at the respective N- and C-terminal tails. The ShA variant presents a long inactivation "chain" at the N-terminus and a short clustering "chain" at the C-terminus and is thus termed $I_LC_S$. Similarly, the ShB, ShD, and $ShD_2$ wild-type channels are termed $I_LC_L$, $I_SC_L$, and $I_SC_S$, respectively. For clarity, the native inactivation and clustering "ball and chain" modules are colored gray and black, respectively. Note that the $I_SC_L$ and $I_SC_S$ (ShD and ShD2) variants carry a different inactivation "ball" than do the $I_LC_S$ and $I_LC_L$ variants (indicated by the white-lined gray "ball"). (c) The six "chain"-level chimeric channels used in the current study to address analogy between the clustering and fast inactivation "ball and chain" mechanisms. Chimeric channels were generated by replacing either the inactivation or clustering "chain" with the short or long native "chain" from the other end of the channel. In all chimeric channels, the original "ball" motif remained intact, thus ensuring that inactivation and clustering occurred at the appropriate N- or C-terminal end. A similar inactivation "ball" was used in all measurements (that of ShA and ShB proteins) thus allowing the assessment of "chain" length effects alone. Chimeric channel nomenclature is read in the N- to C-terminal direction and is based on the identity of the original "chain," whether for a clustering (C) or inactivation (I) "chain" (see text).

metaphor, N- or C-"chain" length, as possibly determined by alternative splicing, for example, provides the time dimension, or the hands of the clock.

The similar "chain" length-dependent binding of either "ball" to its receptor site suggests that the unrelated inactivation and clustering functions of the *Shaker* channel both rely on a similar "ball and chain" mechanism [21,24]. Still, two noteworthy criticisms can be raised when considering this proposed analogy. The first is that these binding metaphors were proposed based on a series of non-natural bulk deletions in either the N- or C-terminal tails. The second concern is that while the "ball"–receptor inactivation binding reaction is intra-molecular, the binding of the channel to PSD-95 is inter-molecular and diffusion limited. This difference affects the effective local concentration of the "ball" near its receptor site, as reflected in the magnitude and type of forward binding rate constants [21]. These reservations thus call for a more detailed analysis of the proposed analogy using direct means.

To determine whether the N- and C-terminal cytoplasmic tails of the *Shaker* Kv channel indeed both rely on a "ball and chain" mechanism to regulate channel inactivation and clustering, we exploited the fact that alternative splicing of the *Shaker* Kv channel gene only occurs at either the N- or C-terminal "chains" to produce natural variants presenting different "chain" lengths [26,27]. These N- or C-terminal variants exhibit length-dependent effects on channel inactivation [14,15,21] and channel binding to PSD-95 [20], respectively, thus highlighting the physiological relevance of the proposed "ball and chain" mechanisms for each event [24]. In the present study, we relied on these naturally occurring long and short N- or C-terminal *Shaker* channel "chains" as the basis for a chimeric channel approach to address whether the fast inactivation and clustering mechanisms are truly analogous. We argue that if "chain"-level chimeric Kv channels in which either the wild-type N-terminal inactivation or C-terminal clustering chain sequences was replaced with natural "chain" sequences originating from the other end of the molecule can support channel inactivation or clustering (as appropriate) in a length-dependent manner, this would be clearly indicative of the unrelated inactivation and clustering Kv channel functions occurring according to a similar "ball and chain" binding mechanism.

## Results and Discussion

### A native "chain"-level chimeric channel approach

In the current study, we focused on four natural channel variants known as ShA, ShB, ShD, and ShD2, representing all four possible combinations of two long and two short natural N- or C-terminal tails [26,27]. The ShA and ShB channel variants share an identical long N-terminal inactivation "ball and chain" sequence, yet present short and long C-terminal clustering "chains," respectively, both terminating with an identical clustering "ball." The ShD and ShD2 variants, on the other hand, carry the short N-terminal inactivation "chain" variant and bear the same C-terminal clustering chains as in the ShB and ShA variants, respectively. A schematic representation of all four variants is presented in Fig. 1b, with the sequences of the long and short inactivation or clustering chain variants provided in SI Fig. 1a. We subsequently renamed these four wild-type-derived channels based on the identity of their terminal inactivation (I) or clustering (C) "chains" (from the N- to the C-terminal) as $I_LC_S$ (ShA), $I_LC_L$ (ShB), $I_SC_L$ (ShD), and $I_SC_S$ ($ShD_2$), with the subscripts S and L designating the short and long native "chain" versions, respectively.

In addition to these four channel variants, six more chimeric channels were generated by replacing either the N- or C-terminal inactivation or clustering "chain" with the short and long native "chain" versions from the other end of the channel, while leaving the appropriate inactivation or clustering "ball" intact (Fig. 1c). The $C_SC_S$ and $C_LC_L$ "chain" chimeras correspond to inactivation chimeras and were generated by introducing one of the two native wild-type clustering "chains" found at the C-terminal end (i.e., $C_S$ or $C_L$) at the N-terminal end, thus replacing the original N-terminal inactivation "chain." Similarly, the $I_LI_S$ and $I_LI_L$ channels correspond to clustering chimeras in which either the short or long native N-terminal inactivation "chain" replaced the original C-terminal clustering "chain." We further generated a $I_LC_L^R$ channel variant in which the long C-terminal chain presents the reversed amino acid order ($C_L^R$). Finally, a $C_L^RC_L$ inactivation chimera was generated in which the $C_L^R$ "chain" was introduced at the N-terminal end adjacent to the original inactivation "ball." These last two channel variants served as internal controls to address the impact of "chain" length on clustering or inactivation, respectively. Here, protein chains presenting identical lengths and amino acid composition (e.g., the $C_L^R$ and $C_L$ "chains") yet different residue order were employed. The sequences of both the N- and C-terminal ends of each chimeric variant are given in SI Fig. 1b.

### Native inactivation "chains" bind PSD-95 via a "ball and chain" mechanism

We initially examined whether the short and long native inactivation "chains" can support channel binding to PSD-95 and, if so, by what mechanism. Ideally, such measurements should be performed in a membrane context, involving the full-length $I_LI_S$ and $I_LI_L$ C-terminal chimeric channels and the cytoplasmic PSD-95 protein. In the absence of such a quantitative experimental setup, we took a reductionist approach and instead studied the abilities of the isolated $I_S$ and $I_L$

inactivation "chains" fused to the PDZ-binding motif clustering "ball" to bind the PDZ domains of PSD-95 in a membrane-mimicking context. First, however, we verified that the $I_S$ and $I_L$ inactivation "chain", previously deduced to be random chains solely on the basis of elegant functional inactivation measurements [14,15], are indeed intrinsically disordered [28], as further predicted by the FoldIndex sequence-based prediction algorithm (SI Fig. 2a) [29]. To verify these predictions, we employed a variety of hydrodynamic and spectroscopic approaches. Size exclusion chromatography revealed that both proteins migrate unusually fast for their actual molecular weights (SI Fig. 2b). Based on a calibration curve generated using protein standards of known molecular weight, much greater Stokes radii were calculated for both the $I_S$ and $I_L$ protein "chains" than what was expected according to their actual sizes (SI Fig. 2c; compare the gray and red data points). This anomaly is not a result of $I_S$ or $I_L$ oligomerization, as analytical ultra-centrifugation analysis revealed a mono-dispersed population for both proteins, with the appropriate expected molecular mass in each case (SI Fig. 2d). We thus conclude that the $I_S$ and $I_L$ protein chains each assume an extended, non-globular shape. Accordingly, the far-UV CD spectrum for each protein lacked the typical signature of $\alpha$-helix and $\beta$-sheet secondary structure elements and exhibited a negative peak at 200 nm, indicative of a strong contribution from disordered elements, characteristic of a protein in a random coil conformation (SI Fig. 2e). NMR analysis further provided evidence that both proteins lack tertiary structure. The $^1$H NMR spectra of both the $I_S$ and $I_L$ inactivation chains (SI Fig. 2f) are typical of intrinsically disordered proteins, lacking the chemical shift dispersion seen with folded proteins. Taken together, our results confirm that the short and long inactivation "chain" variants of the Shaker Kv channel are indeed intrinsically disordered random chains, as previously shown for their long and short clustering "chain" counterparts [19,20].

The isolated $I_S$ and $I_L$ "chains" can, nonetheless, bind the PDZ domains of PSD-95. As seen in Fig. 2, depicting results obtained using a pull-down experimental setup that mimics the native membrane context of the clustering "chains" (Fig. 2a) [20], we found that bead-linked $I_S$ and $I_L$ inactivation "chains" were able to capture the $PDZ_{1,2}$ module of the PSD-95 protein, comprising the first two PSD-95 PDZ

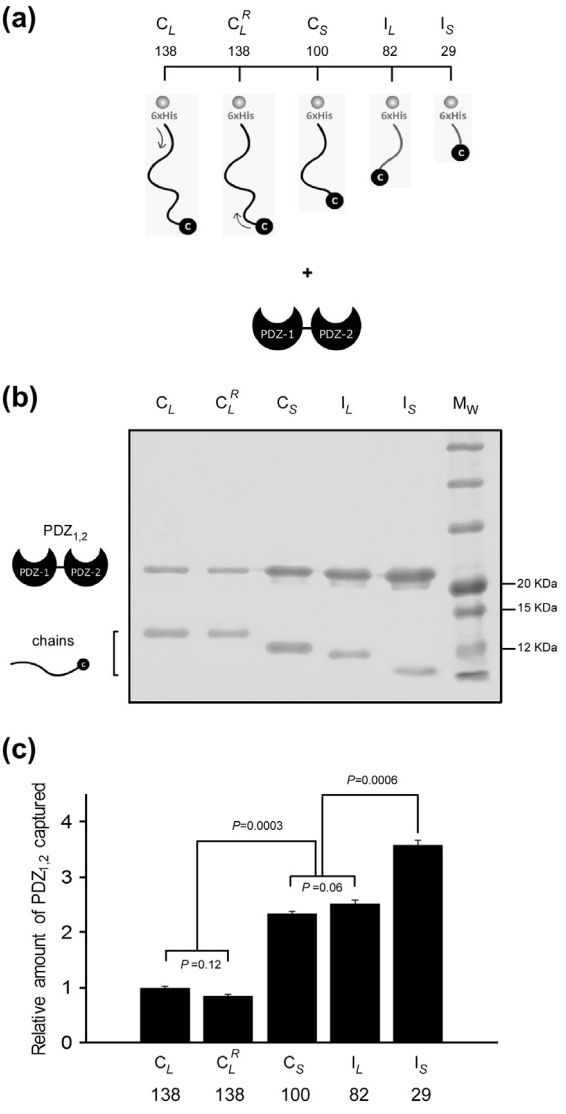


**Fig. 2.** The long and short native inactivation "chains" of the *Shaker* Kv channel support PSD-95 binding in a length-dependent manner. (a) A batch mode pull-down experimental setup for analyzing the binding of isolated long and short native clustering and inactivation "chains" to PSD-95 $PDZ_{1,2}$ domains. The native inactivation and clustering "chains," all harboring the terminal PDZ-binding clustering "ball" (black circle) were bound to $Ni^{2+}$-NTA beads and challenged with identical concentrations of the $PDZ_{1,2}$ protein (see Methods). The isolated "chains" were designated based on their origin, namely clustering (C) or inactivation (I) "chains," with the subscript denoting the short (S) or long (L) "chain" versions. The $C_L^R$ "chain" is similar to the $C_L$ "chain" in both length and composition yet presents a reversed amino acid order. Numbers next to each channel notation indicate C-terminal "chain" length. (b) SDS-PAGE analysis of eluted fractions used to evaluate the amount of $PDZ_{1,2}$ protein captured in each case. (c) Densitometric analysis of the $PDZ_{1,2}$ elution bands plotted as a function of the length of the Kv channel native clustering or inactivation "chain." Mean differences in the amount of $PDZ_{1,2}$ captured by each "chain" ($n$ = 3–5), relative to wild-type $C_L$ chain, were judged for statistical validity, based on a two-tailed Student's $t$ test corrected for multiple comparisons (Bonferroni's correction) and assuming a $p$ value smaller than 0.01 to reject the null hypothesis. Note that the $I_L$ and $C_S$ chains bearing relatively similar "chain" lengths (82 and 100, respectively) captured similar amounts of PDZ domains ($p$ = 0.5). Error bars represent SEM values.

domains (Fig. 2b). Furthermore, comparison of such binding to that seen with the native $C_S$ and $C_L$ clustering "chains" and the $C_L^R$ "chain" revealed a monotonic dependence on chain length (Fig. 2b–c), such that the shorter the native chain, the higher was the amount of $PDZ_{1,2}$ captured. Differences among the "chain"-length variants, relative to the wild-type $C_L$ "chain," were judged for statistical validity using Student's *t* test corrected for multiple comparisons and assuming a *p* value smaller than 0.01 to reject the null hypothesis. The results imply that "chain" length is a major factor controlling binding affinity. In particular, it should be noted that the $C_L$ and $C_L^R$ natural and reversed-order "chains" captured almost identical amounts of $PDZ_{1,2}$, pointing to the seeming unimportance of "chains" orientation with respect to the clustering "ball." To conclude, when attached to the C-terminal clustering "ball," the native inactivation "chains" support PSD-95 binding in a "chain length"-dependent manner, implying that these chains function according to a "ball and chain" mechanism.

As discussed above, a "ball and chain" binding mechanism requires the "chain" to function as an entropic clock that times the binding event [20,24]. Such a mechanism bears unique thermodynamic signatures [24]. First, the affinity between the binding partners should depend on "chain" length in a linear manner. Second, "chain" length should only affect the association kinetics of the "ball" to its receptor site, revealing a power law dependence of the association rate and "chain" length [21]. Furthermore, no effect of "chain" length on the kinetics of complex dissociation is expected. This is manifested by the invariance profile of the association and dissociation rate constants. Determining whether native inactivation "chain"–PDZ interactions indeed adhere to such "ball and chain" signatures thus requires knowledge of the rate and equilibrium constants ($k_a$, $k_d$, and $K_D$) of "chain" binding to PSD-95 PDZ domains. We thus performed surface plasmon resonance (SPR) analytical binding analysis. Typical SPR sensograms describing interactions of the second PSD-95 PDZ domain ($PDZ_2$) with the isolated natural inactivation and clustering chains, all carrying the 6-amino-acid-long PDZ-binding motif clustering "ball", are shown in SI Fig. 3. For all interactions examined, clear association and dissociation phases are apparent. Sensograms of each channel "chain" (at all concentrations tested; see SI Fig. 3 legend) were globally fitted to a modified Langmuir isotherm describing a protein–protein association model involving encounter complex formation followed by an induced fit rearrangement step, as previously reported [20,30]. Estimates for $k_a$, $k_d$, and $K_D$ describing the interactions between $PDZ_2$ and the different native "chain" variants are listed in Table 1. As can be seen in Fig. 3a, both the $I_S$ and $I_L$ chains adhered to the expected linear correlation between the affinity of the two proteins [manifested by association binding energy ($\Delta G = -RT\ln K_A$)] and "chain" length. In particular, the short inactivation "chain" variant exhibited higher affinity for $PDZ_2$ than did the longer variant, whereas both revealed higher affinity, as compared to the longer clustering "chain" variants. Furthermore, in accordance with the results of the pull-down analysis, an almost identical affinity to the PDZ domain was obtained for the $C_L$ and $C_L^R$ chains. Again, these chains are identical in length and composition but oppositely oriented. The results clearly indicate that the inactivation chain-PDZ binding reaction is entropy controlled, thus fulfilling the first signature characteristic of a "ball and chain" mechanism.

We next compared the kinetics of association and dissociation of the different native channel tails to $PDZ_2$ (Fig. 3b–d). The normalized SPR response of all four natural *Shaker* chains as a function of time at identical chain concentrations (12.5 nM) is shown in Fig. 3b. Clearly, major differences between the chains were seen during association, with the shorter the "chain," the faster being the association kinetics. Only minor changes in the dissociation kinetics of the different "chain"–$PDZ_2$ complexes were observed over time (Fig. 3b and Table 1). In fact, the association kinetics of the $C_L$ and $C_L^R$ chain clustering variants to $PDZ_2$ are almost identical. The kinetic behavior observed in

**Table 1.** Rate and equilibrium constants for the native inactivation and clustering "chain" binding to PSD-95[a]

| Spliced "chain" variant[b] | "Chain" length | $k_a$ ($M^{-1}$ $s^{-1}$) × $10^5$ | $k_d$ ($s^{-1}$) × $10^{-2}$ | $K_D$ (× $10^{-8}$)[c] | $\Delta G$[d] (kcal/mol) |
|---|---|---|---|---|---|
| $I_S$ | 29 | 23.00 ± 0.17 | 2.46 ± 0.02 | 0.41 ± 1.51 | −11.28 ± 0.26 |
| $I_L$ | 82 | 16.60 ± 0.04 | 2.67 ± 0.16 | 1.55 ± 2.28 | −10.50 ± 0.29 |
| $C_S$ | 100 | 12.55 ± 0.09 | 3.67 ± 0.02 | 2.97 ± 4.14 | −10.12 ± 0.07 |
| $C_L$ | 138 | 2.89 ± 0.01 | 1.33 ± 0.03 | 5.52 ± 6.50 | −9.76 ± 0.24 |
| $C_L^R$ | 138 | 2.67 ± 0.01 | 1.25 ± 0.01 | 6.64 ± 6.60 | −9.65 ± 0.34 |

[a] Values reported in this table were derived from SRP binding studies conducted at room temperature (25 °C). Values represent the averages of 3–5 independent experiments. Error bars represent error propagation values derived from the multiple experimental errors of the individual measurements.
[b] All native "chains" carried the same 6-amino-acid-long PDZ-binding motif.
[c] Values for the dissociation equilibrium constant were calculated by averaging the $k_d/k_a$ ratio from 3–5 experiments.
[d] Values for $\Delta G$ were calculated according to $\Delta G = -RT\ln K_A$, where $K_A$ is the equilibrium association binding constant between the appropriate "chain" and the $PDZ_{1,2}$ PSD-95 protein fragment.

Fig. 3b is independent of chain concentration (not shown) and is further manifested in the log$k_d$ *versus* log$k_a$ plot (Fig. 3c), demonstrating the invariance between the two quantities. Whereas $k_a$ values for the longer and shorter channel "chains" varied by an order of magnitude, protein dissociation (once the complex had formed) was independent of "chain" length, as revealed by the similar $k_d$ values obtained for all chains. Finally, plotting the normalized association rate constants of native inactivation and clustering variants together with those of C-terminal artificial deletion "chain" variants as a function of "chain" length difference ($\Delta N$) revealed a power law dependence (Fig. 3d) [20]. Fitting the data to a theoretical "random walk"-based equation, derived assuming a pure "ball and chain" mechanism [21] (Eq. (2); see Methods), revealed a power law value of 1.46 (±0.01), almost identical to the 3/2 value expected by theory (black curve; $R^2$ =0.88).

Taken together, the results clearly reveal that the native inactivation "chains" fused to the clustering "ball" function as entropic clocks to time PDZ binding, as do the native clustering "chains". The native inactivation "chain"-PSD-95 binding reactions thus fulfill the thermodynamic signature of a "ball and chain" mechanism involving entropic random chains [20,21].

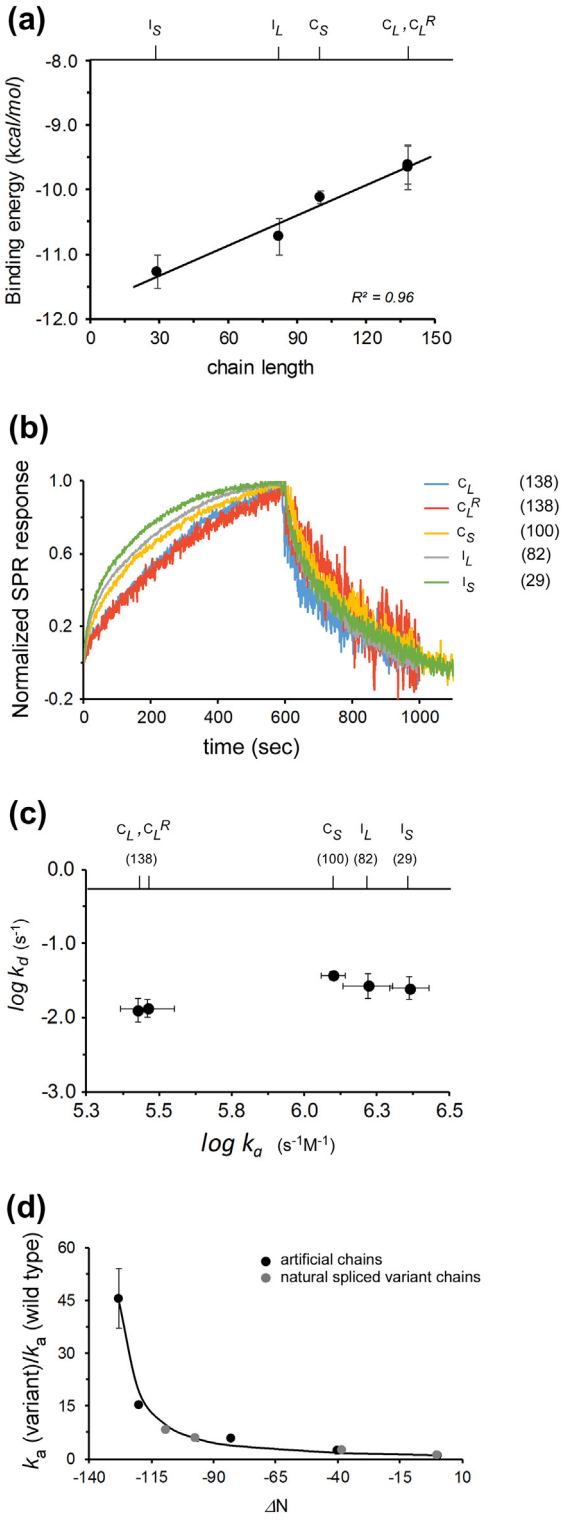


**Fig. 3.** Native inactivation "chains" support Kv channel binding to PSD-95 according to a "ball and chain" mechanism. (a) Plot of the association binding energy ($-RT\ln K_A$) between natural clustering or inactivation *Shaker* Kv channel "chains" and the $PDZ_2$ PSD-95 protein fragment, as a function of "chain" length. The solid curve corresponds to a linear regression ($R^2$ = 0.96). Experiments were carried out using SPR binding analysis (SI Fig. 3; see Methods) and were repeated 3–5 times at 25 °C. Estimates for $K_D$, $k_a$, and $k_d$ for each native chain–$PDZ_2$ interaction were obtained upon global fitting of the SPR sensograms to a Langmuir isotherm describing protein–protein association kinetics (see Methods) [30] and are reported in Table 1. (b) Comparison of the normalized association and dissociation kinetics of the natural short and long inactivation or clustering "chain" variants to and from $PDZ_2$, respectively. For each trace, identical concentrations of $PDZ_2$ and native channel "chains" (2 μM) were used and the curve was normalized relative to the maximal response noted at the end of the association phase. (c) Association–dissociation rate constant correlation plot of the native "chain"–$PDZ_2$ interaction. Numbers on the upper horizontal axis indicate native "chain" length. (d) Dependence of the scaled native "chain"–$PDZ_2$ association rate constant ($k_a/k_a$reference (*ShB*)) on "chain" length difference ($\Delta N$). Gray data points represent artificial "chain" deletions, whereas black points refer to native "chain" replacements. The solid line represents the best fit of the data to Eq. (2) (see text) describing a random flight "ball and chain" mechanism for channel binding to $PDZ_2$. In all panels, error bars represent standard errors, a result of error propagation of the values obtained from 3–4 experiments.

## Native inactivation "chains" support PSD-95-mediated channel clustering

We next addressed whether native inactivation "chains" support cellular PSD-95-mediated mem-

brane surface channel expression and clustering *in vivo*, using a protocol previously employed for studying clustering [20]. Confocal microscopy was used to image embryonic *Drosophila* Schneider cells transfected to express mCherry-tagged wild-type $I_LC_S$ and $I_LC_L$ channels or their $I_LI_L$ and $I_LI_S$ C-terminal chimeric inactivation counterparts, either alone or together with a PSD-95-GFP fusion protein (see Methods). Typical images for each case are presented in Fig. 4. Control experiments involving cells transfected to express either the wild-type or individual chimeric channels showed no or very minor channel localization at the plasma membrane (Fig. 4a; some plasma membrane localization is observed for the $I_LI_S$ construct). Instead, the different channel proteins were detected throughout the cytoplasm. However, co-expression of the *Shaker* channel chimeric variants together with PSD-95-GFP resulted in channel membrane surface expression and clustering, as well as PSD-95-membrane association, as respectively reflected by the *Shaker* channel-associated red fluorescence (Fig. 4b, left images) and the PSD-95-GFP-based green fluorescence patterns (Fig. 4b, middle images). The yellow coloring of the merged images (Fig. 4b, right images) reveals the overlap of the clustered wild-type or chimeric channels and PSD-95, reflecting the protein co-localization underlying channel surface expression and clustering. In all cases, channel clustering was reflected by a speckled co-localization pattern. This array of co-localization sites probably reflects mega-clustering sites with areas in the sub-$\mu m^2$ range [20], the result of fusion of many smaller clustering sites. Thus, chimeric channels presenting entropic inactivation "chains" at the C-terminus can support PSD-95-mediated cell surface channel expression and clustering.

## Kv channel C-terminal "chain" length affects PSD-95-mediated channel clustering

Do wild-type or variant channels carrying C-terminal "chains" of different lengths exhibit differences in PSD-95-mediated clustering patterns? Such differences can be qualitatively seen upon inspection of Fig. 4b. For example, the $I_LC_L$ channel protein bearing the longest C-terminal "chain" of all channel variants presents a speckled pattern of small-sized clusters, as compared with the $I_LI_S$ variant bearing the shortest C-terminal

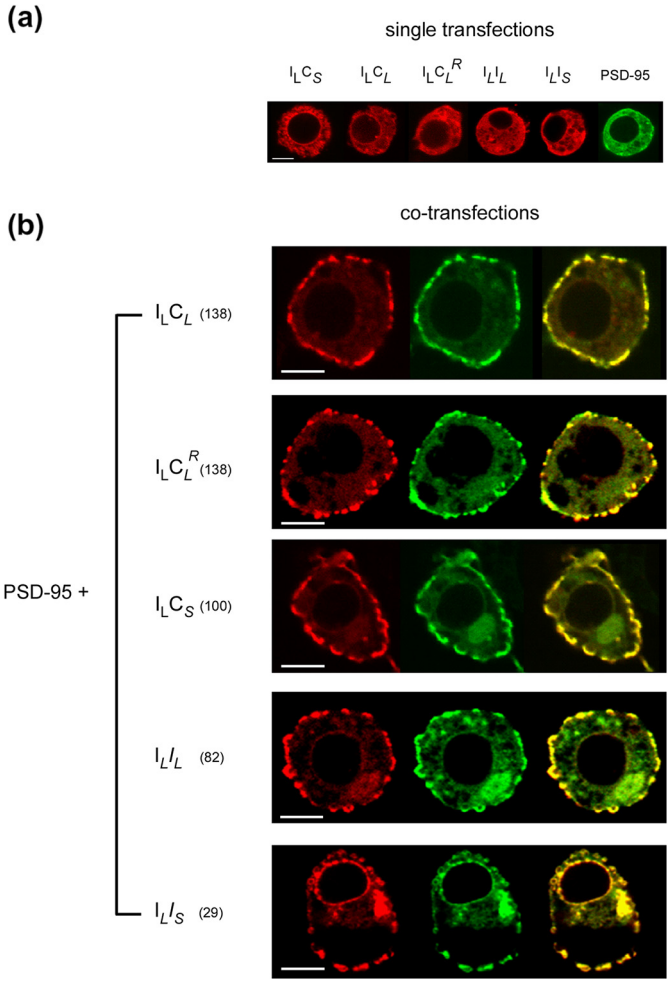


**Fig. 4.** Native inactivation "chains" support PSD-95-mediated Kv channel membrane surface expression and clustering. (a) Confocal microscopy analysis of *Drosophila* S2 Schneider cells expressing either the PSD-95-GFP fusion protein or native or "chain"-level chimeric mCherry-tagged *Shaker* Kv channels alone (see Methods). (b) Typical confocal microscopy analysis of *Drosophila* S2 Schneider cells co-expressing PSD-95-GFP and either a native channel ($I_LC_S$ or $I_LC_L$) or a chimeric channel variant ($I_LC_L^R$, $I_LI_L$, or $I_LI_S$). For each cell, three images are shown, with the red channel-associated and green PSD-95-associated fluorescence signals presented in the left and middle columns, respectively. The merged image of each cell is shown in the right column. Scale bars in panels a and b correspond to 2 μm. Numbers aside each channel notation indicate C-terminal amino acid "chain" length.

"chain." To answer the question above, we used the clustering metrics methodology we previously described [20], and examined whether the different wild-type or chimeric channel proteins revealed differences in mega-cluster area size. Briefly, the yellow speckled co-localization signal along the plasma membrane of cells expressing each channel variant along with PSD-95 ($n = 10–12$) was sampled and used to automatically select all mega clustering sites with accurately defined borders (see Methods). The areas of all membranous clusters were then calculated and recorded. Overall, ~100–250 clusters were analyzed for each variant. The results, comparing the distributions of cluster area sizes, mean number of clusters per cell, and mean cluster area sizes of all variants, are presented in Fig. 5 and SI Fig. 4. The distributions of the mega-cluster area sizes of all "chain"-length variants presented different shapes (SI Fig. 4). For example, the cluster area size distribution of the $I_LI_S$ channel bearing the shortest C terminal "chain" (29) is skewed to the right along the area size axis, as compared to the long "chain" bearing $I_LC_L$ distribution (138 amino acids; Fig. 5a). On the other hand, the cluster area size distributions of the $I_LC_L$ and $I_LC_L^R$ channels presenting an identical "chain" length (138 aa) seem similar (SI Fig. 4). Statistical significance of these differences was examined using the Kolmogorov–Smirnov non-parametric test and sequential Bonferroni correction (see Methods). *p* Values for all distribution pairwise comparisons were found to be smaller than 0.001, but not for the $I_LC_L$ and $I_LC_L^R$ channel pair ($p = 0.52$). Quantitative analysis of cluster area size distributions of all variants revealed interesting observations. First, no difference was observed in the mean number of (mega-) clusters per cell among the different channel variants (Fig. 5b; $n = 10–12$; $p$ values greater than 0.1 were obtained for all pairwise comparisons using an ANOVA test). Second, the different C-terminal "chain"-length variants exhibited differences in mean cluster area size as can be further judged by the Wald $chi^2$ statistical test (Fig. 5c; see Methods). Third, no differences in the mean cluster area size were observed for channel pairs of identical "chain" lengths ($I_LC_L$ and $I_LC_L^R$) or for the $I_LI_L$ and $I_LC_S$ channel pair, which presents relatively similar C-terminal "chain" lengths (82 and 100 amino acids, respectively; Fig. 5c). Last, and most interesting, an inverse linear correlation was observed between the mean cluster area size of the different channel variants and C-terminal "chain" length, with the shorter the terminal "chain," the bigger was the mean mega-cluster area size (Fig. 5d). Taken together, our results reveal that short "chain" high-affinity channel variants support clusters of larger areas than do long "chain," low-affinity variants, thus establishing a direct link between channel C-terminal "chain" length and (mega-) cluster area size. This principal observation thus hints at the cellular correlate of the "ball and chain" molecular mechanism. Further investigation, however, is needed to rationalize the observed linear correlation between the two quantities.

## Native clustering "chains" support channel inactivation via a "ball and chain" mechanism

In the coming paragraphs, we describe complimentary experiments aimed at determining whether native clustering "chains" can be used instead of the original inactivation "chains" to support channel fast (Ns before,-type) inactivation in a length-dependent manner, as would be expected in a "ball and chain" mechanism. Specifically, these experiments examined the kinetics of channel fast inactivation of the $C_SC_S$, $C_LC_L$ and $C_L^RC_L$ inactivation chimeras (Fig. 1c) and compared the values obtained to those presented by the wild-type $I_LC_S$, $I_LC_L$ and $I_SC_L$ channels (Fig. 1b). The six wild-type or variant channels considered here comprise a protein series with increasing N-terminal "chain" lengths, ranging from 29 ($I_SC_L$) to 41 ($I_LC_S$ and $I_LC_L$) to 100 ($C_SC_S$) and up to 138 amino acids ($C_LC_L$ and $C_L^RC_L$), all ending with the same inactivation "ball" (that of *Shaker* A and B). As before, this channel series contains two channel pairs with identical N-terminal chain lengths, thus allowing for an internal control. DNA encoding the wild-type or chimeric channels listed above was transcribed *in vitro* and the resulting mRNAs were injected into *Xenopus laevis* oocytes. For all wild-type and variant channels, fast inactivation kinetics was conventionally monitored using two-electrode voltage clamp electrophysiology recordings (SI Fig. 5 and Fig. 6). For all channel variants, fast inactivation kinetics was measured at various depolarizing voltages by applying a square pulse voltage command protocol (SI Fig. 5a) and monitoring of the resulting potassium currents flowing through the channel (SI Fig. 5b). The inactivation data were fitted to a double exponential function, as commonly done [16,31,32], to yield estimates for the time constants of the fast and slow components of the inactivation process for each channel protein. Following others, we only considered the fast component that is typically responsible for more than 85% of current amplitude (see Methods; SI Fig. 5b) [16]. The dependence of the fast component of each channel protein on voltage is presented in SI Fig 5c.

To examine whether the inactivation process is "chain"-length dependent, inactivation traces of the wild-type or chimeric channels should be compared at an identical voltage. We chose a test value of +40 mV for such comparison as at this voltage, the probability of *Shaker* channels to be open is near 0.9 [12,13] and because this value resides within the voltage range at which leveling off is observed for the voltage-dependence of channel inactivation (SI Fig. 5c). Normalized inactivation currents at +40 mV, measured relative to the maximal peak currents in each case, are shown in Fig. 6a, with the corresponding inactivation time constant ($\tau$) of each channel protein compared in

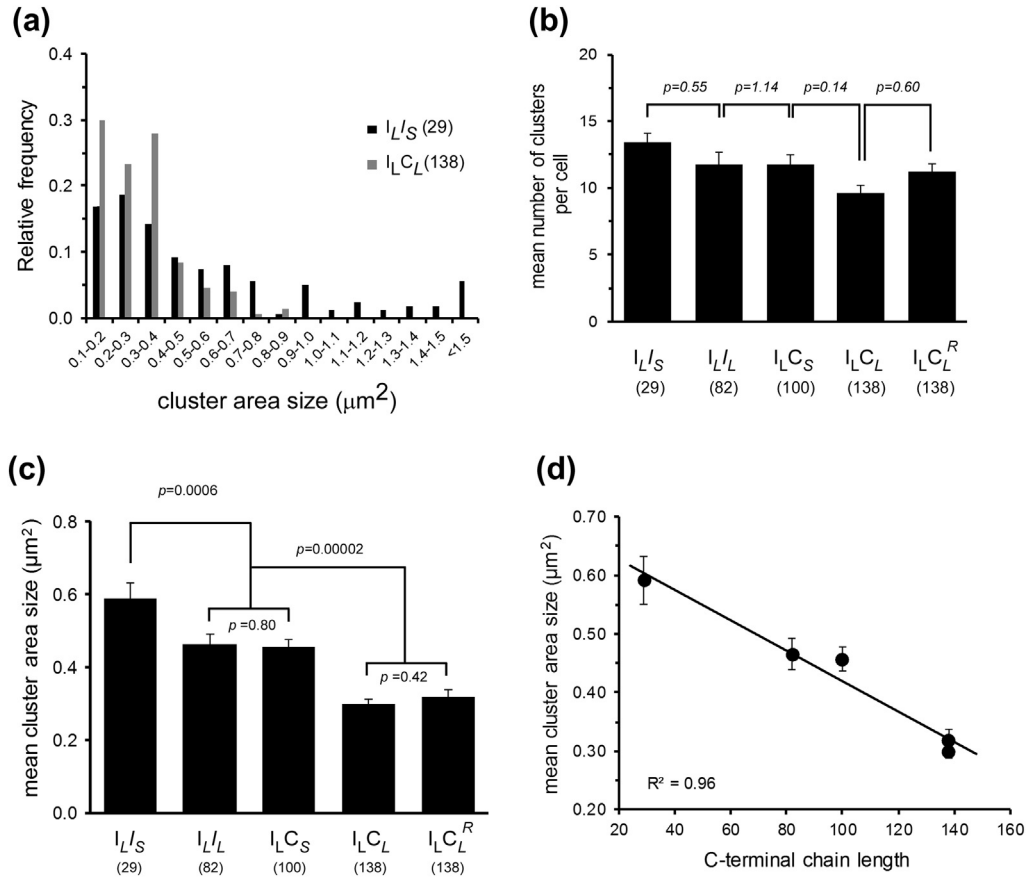


**Fig. 5.** Kv channel C terminal "chain" length affects PSD-95-mediated channel clustering. (a) Mega cluster area size distributions of the $I_LC_L$ and $I_LI_S$ channel variants, as supported by PSD-95. Distributions in steps of 0.1 $\mu m^2$ are presented. (b) Comparison of the mean number of plasma membrane-associated channel clusters per cell ($n = \sim 10–12$ cells; $p > 0.1$ for all pairwise comparisons in an ANOVA test). (c) Comparison of mean area size of channel variant clusters. Differences were judged for statistical validity based on a Wald $\chi^2$ test (see Methods) and assuming a $p$ value smaller than 0.01 to reject the null hypothesis ($n = 100–250$). (d) Dependence of the mean cluster area size of the different channel variants on C terminal "chain" length. Error bars in the appropriate figure panels represent SEM values. The solid curve corresponds to a linear regression with $R^2$ value of 0.96.

Fig. 6b. Several points are worth noting. First, all N-terminally inserted clustering chains supported fast channel inactivation (Fig. 6a, gray traces). Second, the inactivation time constants measured for the wild-type *Shaker* A and B channel variants ($I_LC_S$ and $I_LC_L$, respectively) were similar to those previously reported (Fig. 6b) [31,32]. Third, channels presenting N-terminal "chains" of different lengths revealed differences in inactivation time constants, as validated based on a Student's $t$ test corrected for multiple comparisons (Fig. 6b). Furthermore, both of the wild-type and chimeric channel pairs presenting identical N-terminal "chain" lengths (i.e., the $I_LC_S$ and $I_LC_L$ and the $C_LC_L$ and $C_L^RC_L$ pairs) exhibited similar inactivation time constants, as further judged by the $p$ values of their comparisons being greater than 0.3 (Fig. 6b). Last, clear length dependence was observed for the kinetics of channel inactivation. In other words, the longer the N-terminal "chain," the slower were the fast inactivation kinetics (Fig. 6b).

Does the fast inactivation gating transition of the wild-type and chimeric channel variants indeed adhere to the "ball and chain" mechanism? To answer this question, one needs information on the values of the elementary rate constants for entry into ($k_{on}$) and recovery from ($k_{off}$) inactivation. For this purpose, we assumed a single inactivation gating transition, to a first approximation (see Methods), and used both $\tau$ ($= 1/(k_{on} + k_{off})$ and the normalized steady-state amplitude factor ($= I_{ss}/I_{peak} = (k_{off}/(k_{on} + k_{off}))$ to derive approximations for $k_{on}$ and $k_{off}$ for the different wild-type or chimeric channels. The values for $k_{on}$ and $k_{off}$ are reported in Table 2 and further analyzed in Fig. 6c–d. Several points are noted. First, changes in the $k_{on}$ values of the different channel chains are almost 2 orders of magnitude in

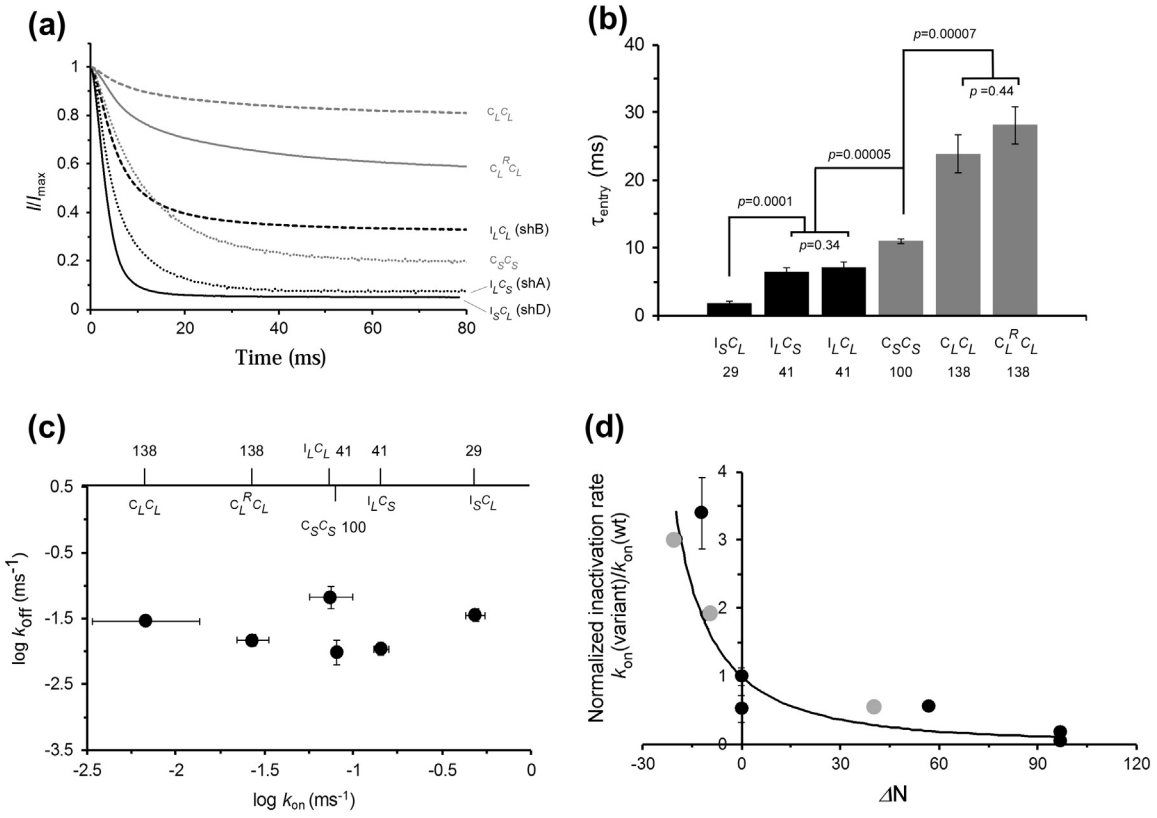


**Fig. 6.** Native clustering "chains" support Kv channel fast inactivation according to a "ball and chain" mechanism. (a) $K^+$ currents recorded from *X. laevis* oocytes expressing wild-type (black) or chimeric (gray) Kv channels (all bearing the same inactivation "ball") in response to a square pulse from a holding potential of −110 mV to +40 and back. Potassium currents through each channel protein were normalized relative to the appropriate peak current. (b) Bar graph depicting the inactivation time constant (τ) of the measured wild-type and chimeric channel proteins obtained by fitting the data presented in a to a double-exponential function (see Methods). Differences in time constants between "chains" of different lengths were judged for statistical validity based on an unpaired Student's *t* test and a Bonferroni correction for multiple comparisons and assuming a *p* value smaller than 0.001 to reject the null hypothesis. Error bars for the different channel constructs represent standard error of the mean using *n* samples ranging from 12 to 20. (c) correlation plot relating the backward ($k_{off}$) and forward ($k_{on}$) inactivation rate constants of the different wild-type or inactivation chimera channel proteins (Table 2). Numbers on the upper horizontal axis indicate "chain" length. (d) Dependence of the scaled forward inactivation rate constant ($k_{on}/k_{on\ reference\ (ShA)}$) of native wild-type channels, inactivation chimeric channels (both in black symbols) and "chain" deletion or insertion mutants (gray symbols) on the "chain" length difference (Δ*N*). The solid line represents the best fit of the data to Eq. (2) (see Methods and text), describing a random flight "ball and chain" mechanism for channel fast inactivation.

size (Table 2). Compared to this change, differences in $k_{off}$ of the different channels are relatively minor. Second, the $k_{on}$ values of the different channel proteins exhibit "chain length" dependence, with the shorter the "chain," the faster was the onset of inactivation kinetics. No such dependence was observed for the $k_{off}$ inactivation rate constant (Table 2). These latter two points are further manifested in the log$k_{off}$ *versus* log$k_{on}$ plot (Fig. 6c), demonstrating the invariance between the two quantities. Third, plotting the forward rates of channel entry into inactivation for the different N-terminal channel "chains" (normalized relative to the wild-type ($I_LC_S$ channel), as a function of chain length difference (Δ*N*), as previously performed when deletions in chain length were considered [21] (shown as gray symbols and measured using a similar voltage step), again revealed a monotonic power law dependence of the $k_{on}$ ratio on Δ*N* (Fig. 6d). The chimeric and deletion channel $k_{on}$ data were together fitted to Eq. (2). As can be seen, the data set is reasonably fitted to Eq. (2) ($R^2$ = 0.80), yielding an estimate for power law dependence (*n*) of 1.82 (±0.23). The estimated *n* value is very close to the 3/2 power law value expected for a "ball and chain" mechanism [21]. Combined, our results demonstrate that the native clustering "chains" can replace the original inactivation "chains" to support

**Table 2.** Forward and backward inactivation rate constants for wild-type and inactivation chimera channel proteins[a]

| Channel variant[b] | "Chain" length[c] | τ (ms)[d] | Amplitude = ($I_{ss}/I_{peak}$) | $k_{on}$ ($ms^{-1}$)[e] | $k_{off}$ ($ms^{-1}$)[e] |
|---|---|---|---|---|---|
| $I_SC_L$ | 29 | 1.91 ± 0.22 | 0.067 ± 0.012 | 0.488 ± 0.051 | 0.035 ± 0.020 |
| $I_LC_S$ | 41 | 6.47 ± 0.54 | 0.069 ± 0.014 | 0.143 ± 0.002 | 0.010± 0.006 |
| $I_LC_L$ | 41 | 7.09 ± 0.85 | 0.469 ± 0.058 | 0.074 ± 0.007 | 0.066 ± 0.040 |
| $C_SC_S$ | 100 | 11.03 ± 0.10 | 0.108 ± 0.014 | 0.081 ± 0.001 | 0.009 ± 0.004 |
| $C_LC_L$ | 138 | 28.14 ± 2.85 | 0.809 ± 0.023 | 0.006 ± 0.0004 | 0.028 ± 0.013 |
| $C_LC_L^R$ | 138 | 23.90 ± 2.77 | 0.067 ± 0.012 | 0.027 ± 0.0004 | 0.014 ± 0.009 |

[a] Measured 16 °C and under a 40 mV depolarizing voltage, as described in the main text and Methods.
[b] The long and/or short "chains" of the wild-type or inactivation chimera proteins all carried the same 20-amino-acid-long inactivation "ball" sequence motif.
[c] "Chain" length was determined in line with reference [14] and excluding the first 20-amino-acid-long "ball" sequence.
[d] Values for inactivation time constants represent the fast component of the inactivation kinetics (see Methods).
[e] Approximations of the values for $k_{on}$ and $k_{off}$ were derived as described in Methods and represent the averages of 8–10 independent experiments. Error bars represent standard errors derived by propagating the SEM values of the time and amplitude constants.

channel fast inactivation in a length-dependent manner, as predicted by a "ball and chain" mechanism involving entropic chains.

## Concluding Remarks

The results reported here provide direct evidence for the analogy between the *Shaker* Kv channel fast inactivation and clustering "ball and chain" mechanisms. Both native spliced variant fast inactivation and clustering "chains" can replace their counterpart "chains," when attached to the appropriate "ball." Specifically, the affinity of the clustering "ball"-bearing inactivation chains to PSD-95 presents the expected linear dependence on "chain" length (Fig. 3a), as brought about by changes in the association rate constant alone (Fig. 3b–c) [24]. Furthermore, the inactivation "chains" adhere to the expected power law dependence of the rate constants for channel-PSD-95 binding on chain length, implying that the inactivation chains, like their clustering counterparts, also time complex formation (Fig. 3d). In the context of the full-length channel, the inactivation "chains" also support PSD-95-mediated *Shaker* channel clustering (Fig. 4) in a length-dependent manner (Fig. 5). At the same time, the clustering "chains" support fast N-type channel inactivation in a length-dependent manner when attached to an inactivation "ball," again as predicted by the "ball and chain" mechanism. Specifically, the scaled entry into inactivation rate constant ($k_{on}$) of the clustering "chains" adheres to the power law dependence on "chain" length difference (Fig. 6d) with a value close to 3/2 obtained using all inactivation and clustering "chains."

Taken together, our clustering and inactivation measurements using native inactivation or clustering "chains," respectively, are in line with those obtained using artificially deleted "chains," with both sets of measurements revealing "random walk"-based, length-dependent binding kinetics. Both mechanisms involve entropic "chains" that do not fold upon binding and only provide the necessary degrees of freedom needed to reach the "ball" receptor site. Furthermore, for both the inactivation and PSD-95 binding processes, whether measured using native or artificial "chains," invariance between the corresponding forward and backwards rate constants is observed (Figs. 3c and 6c herein and Fig. 2d of Ref. [20], respectively), thus exhibiting the expected thermodynamic signature of a "ball and chain" binding mechanism [24]. The analogy between the N- and C-terminal-based "ball and chain" mechanisms is further strengthened if one considers that PSD-95 is *a priori* membrane-associated due to its palmitoylation [33], as well as the observation that the onset of Kv channel fast (N-type) inactivation occurs in a similar manner when the "ball and chain" sequence is carried on the auxiliary β subunit of the channel with which it interacts, and not on the channel itself [34]. Considering this latter variation on the fast inactivation theme argues that both the scaffold protein-binding and the inactivation channel processes are indeed timed by entropic chains that operate according to a similar "ball and chain" mechanism.

## Methods

### Molecular biology and protein expression and purification

The PSD-95 protein used in the current study is the *Drosophila* S97 variant. Cloning of sequences encoding the short and long native N-terminal inactivation "chain" variants fused to the 6-amino-acid-long terminal PDZ-binding motif clustering "ball" ($I_S$ and $I_L$) or the $C_L^R$ chain into the His-tag-encoding pHis parallel vector was performed as described previously [20]. The long inactivation "chain" also included the unstructured linker up to the T1 domain. This allows for an appropriate "chain" length span for the *in vitro* binding analysis (SI Fig. 1). Chimeric channel construction was performed by restriction-free cloning using the *Phusion* polymerase (NEB). For

protein clustering analysis, DNA encoding the full-length wild-type or chimeric *Shaker* Kv channel variants was cloned into the *Drosophila* pUAST vector carrying the reading frame of the mCherry fluorescent protein marker. For channel fast inactivation measurements, DNA encoding the full-length wild-type or chimeric Shaker Kv channel variants was cloned into the pRAT vector. All constructs were verified by sequencing. mRNA for wild-type or chimeric channel was synthesized using T7 RNA polymerase, as previously described [20]. Expression and purification of $I_S$ and $I_L$, $C_L^R$, $PDZ_{1,2,}$ and $PDZ_2$ were performed as previously described [20], as were that of the $C_L$ and $C_S$ native clustering chains.

### Disorder prediction

The intrinsic disorder tendencies of the $I_S$ and $I_L$ fusion "chains" were calculated using the Foldindex disorder predictor (http://bip.weizmann.ac.il/fldbin/findex) [29] based on the mean net charge and hydrophobic properties of the sequence [35]. Predictions were further verified using other servers.

### Size exclusion chromatography

For Stokes radius determination, gel filtration of $I_S$ or $I_L$ and standard molecular weight marker proteins was performed on an analytic size exclusion column (Superdex 200, 10/300), as previously described [20].

### Analytical ultracentrifugation

Equilibrium ultracentrifugation experiments were performed using a Beckman XL-A ultracentrifuge with an An60 Ti rotor at 20 °C, as previously described [20]. A concentrated sample of either $I_S$, $I_L$, or $C_L^R$ was prepared and diluted 1:2 and 1:3 with appropriate buffer to generate final protein solutions of approximately 15, 31, and 63 μM, which were loaded into a six-sector cell and spun at rotor speeds of 19,000 and 21,000 rpm. Data were collected at each speed for each protein concentration ($c$) at 230, 260, 280, and 320 nm and analyzed using the following equation: $M = [2RT/(1 - \ddot{u})\rho\omega^2][(\partial \ln(c))/\partial r^2]$, with $\ddot{u}$ set at 0.73 $cm^3\ g^{-1}$ and $\rho$ at 1.012 g $cm^{-1}$, as calculated using Ultrascan software (http://www.ultrascan.uthscsa.edu) [20].

### Circular dichroism spectroscopy

Circular dichroism (CD) wavelength scan measurements were recorded on a Jasco J-815 model CD spectrometer. All CD spectra were recorded in 10 mM NaCl and 5 mM Tris–HCl (pH 8) with a bandwidth of 2 nm and an averaging time of 1 s. Far-UV spectra were recorded at room temperature using a 1-mm cuvette and $I_S$ and $I_L$ protein concentrations of 0.25 mg/ml. Each spectrum presented is derived from 10 independent spectra, averaged and baseline-corrected for the contribution of the sample buffer.

### $^1$H-NMR spectroscopy

NMR spectra of the $I_S$ and $I_L$ proteins were recorded in a 95% $H_2O$/5% $D_2O$ solvent mixture. Data were acquired on a Bruker 500 MHz spectrometer and analyzed with Bruker XWINNMR software. 1D-$^1$H-NMR spectra were collected at room temperature, and water suppression was achieved using the WATERGATE sequence. Resolution enhancement was achieved by application of a sine-square window function to the free induction decay.

### Pull-down analysis

A batch mode pull-down experimental setup was used to analyze isolated channel "chain" binding to PSD-95 $PDZ_{12}$ domains. Briefly, $Ni^{2+}$ bead-attached long and short native inactivation or clustering "chains" (i.e., $I_S$, $I_L$, $C_S$ $C_L$, or $C_L^R$), each harboring the terminal PDZ-binding motif (SIETDV), were challenged with a $PDZ_{12}$-containing PSD-95 protein fragment. The amount of $PDZ_{12}$ captured in each case was evaluated by SDS-PAGE. Densitometry analysis of the $PDZ_{12}$ elution bands was performed as previously described [20]. The experiment was repeated for 3–5 times. The differences in the amounts of $PDZ_{12}$ captured by each native chain (relative to what was captured by a reference wild-type chain) were averaged and the SEM values are reported. Statistical significance of these differences was judged using the Student's $t$ test with Bonferroni correction for multiple comparisons [36] and assuming a $p$ value smaller than 0.01 to reject the null hypothesis.

### SPR analysis

SPR was performed using a ProteOn XPR36 instrument (BioRad), as previously described. Briefly, a $PDZ_2$ PSD-95 protein fragment was bound to a mass-sensitive GLC chip by passing a solution of 50 μM $PDZ_2$ protein (1 μg in total) in PBST buffer (pH 7.4) over the chip at a flow rate of 100 μl/min. Following binding and washing, different concentrations (0–50 nM) of the native inactivation and clustering "chain" proteins in the same buffer were allowed to flow over the chip. $PDZ_2$-tail binding experiments were repeated 3–5 times at 25 °C.

### Cell culture and transformation of *Drosophila* Schneider cells

Schneider cells (S2R+) were cultured in *Drosophila* Schneider cell medium (Biolabs Industries, Israel) containing 10% fetal bovine serum (Biolabs Industries) and the antibiotics penicillin (0.1 mg/ml), streptomycin

(10 mg/ml), and 0.025 mg/ml amphotericin B solution (1:100; Biolabs Industries). Cells were maintained at 25 °C under a normal atmosphere. For transient transfections, $1 \times 10^6$–$4 \times 10^6$ cells were cultured in 12-well culture plates for 24 h and transfected with 4 μg of either plasmid pUAST-mCherry-Channel or plasmid pUAST-PSD95-GFP or with 4 μg of both in co-transfection experiments, using the TransIT transfection reagent (Mirus). Expression of all pUAST constructs was driven by co-transfection with an actin-Gal4-encoding plasmid. Transfected cells were cultured for 24 h in *Drosophila* medium and fixed 24–48 h later using a fixation reagent.

### Confocal microscopy surface expression and clustering analyses

Assessment of membrane surface expression and clustering of wild-type or chimeric Kv channel variants was performed essentially as previously described [20]. Briefly, the $I_LC_S$ and $I_LC_L$, wild-type channels and the $I_LI_L$, $I_LI_S$ and $I_LC_L^R$ chimeric channel variants were expressed by transfecting *Drosophila* Schneider cells with pUAST-mCherry-wt or chimeric channel fusion plasmids either alone or with the pUAST-GFP-PSD-95 fusion plasmid, as previously described [20]. For examining channel clustering, the cells were fixed with 4% formaldehyde (Sigma) in PBS for 15 min and then washed and mounted in 50% glycerol. Detection of fusion channel and PSD-95 proteins was performed by measuring the respective red and green fluorescence signals. Images were taken at the equatorial focus plane, such that the nucleus exhibited its longest dimension, using a LSM510 Zeiss confocal microscope. Images of mCherry-labeled native $I_LC_S$ and $I_LC_L$ channels or their $I_LI_L$ and $I_LI_S$ C-terminal chimeric inactivation counterparts, either alone or together with a PSD-95-GFP fusion protein are presented in Fig. 4.

### Channel clustering metrics

Channel clustering metrics at the whole-channel level were evaluated by monitoring the co-localization pattern of the channel and PSD-95 proteins at the plasma membrane of Schneider cells using the latest version of the Photoshop software (Adobe CS6 extended version) that includes an image processing measurements module. Briefly, the co-localization yellow signal of the merged images of ~12 different cells was evaluated in the plasma membrane by sampling the yellow-marked membrane clusters signal followed by use of the "Grow" and "Similar" select commands until all membrane clusters were selected and their boundaries exactly defined. Measurements of the area and perimeter of all marked clusters were then automatically recorded. The analysis above was repeated, in a blind manner, yielding similar results to those reported here.

To test whether cluster area size (a dependent variable) differed between the different channel variants (an independent variable), a generalized linear model analysis was performed with Gamma distribution assumed for the cluster area size variable and log link function between the linear predictor and the mean of the distribution function, given how the variant cluster area size distributions appear non-normal. The Wald $\chi^2$ test was used to examined the null hypothesis that the mean cluster area sizes of the different channel variants are the same. Rejection of the null hypothesis was made based on $p$ values smaller than 0.001. To examine whether the shape of the different channel cluster area size distributions differed, the Kolmogorov–Smirnov non-parametric test was employed with sequential Bonferroni correction applied [36].

### Electrophysiology

$K^+$ currents were recorded from the wild-type or chimeric channels under conditions of two-electrode voltage clamp (OC725B, Warner Instruments) 1–3 days after injecting either wild-type or chimeric channel variant mRNA (50 ng), respectively, as described previously [20]. Fast inactivation gating measurements were performed in a bath solution containing (in mM): 93 NaCl, 2.5 KCl, 1 $MgCl_2$, 0.3 $CaCl_2$, and 5 Hepes (pH) 7.4. For assessing the contribution of slow (C-type) inactivation, an external potassium concentration of 160 mM was used. Oocytes were held at a resting membrane voltage of −110 mV, and $K^+$ currents were elicited upon various depolarizing steps ranging from −20 to +50 mV, followed by step repolarization to the holding membrane voltage. All experiments were conducted at 16 °C.

### Data analysis

SPR sensograms were globally fitted to a two-step protein–protein association model involving encounter complex formation, followed by a rearrangement step at the binding interface (induced fit) [30]. This model was found to adequately describe the association kinetics of PSD-95 PDZ domain binding to its peptide ligands [20]. For each channel tail-PDZ pair, adequacy of the global fit was judged based on a $\chi^2/R^{max}$ value smaller than 10%, as commonly accepted. In all cases, the equilibrium constant for the rearrangement step was found to be invariant of chain length, as expected when such isomerization reflects a binding site rearrangement transition. Inactivation kinetics were analyzed using a double-exponential function to yield the amplitude ($A$) and time constant ($\tau$) for both the fast and slow components of the inactivation reaction [31,32]. As in other studies, only the fast component of the inactivation process was considered, as it is the major component

typically responsible for more than 85% of the current amplitude.

Values for the forward and backward inactivation rate constants ($k_{on}$ and $k_{off}$, respectively), corresponding to the major component of the fast inactivation gating transition, were calculated using the inactivation time constant ($\tau = 1/(k_{on}+k_{off})$) and the normalized steady-state amplitude factor ($A_{ss} = I_{ss}/I_{peak} = k_{off}/(k_{on} + k_{off})$, where $I_{ss}$ and $I_{peak}$ are the respective steady-state and peak current levels. These values are reasonable approximations for the true constants, as the contribution of the second phase in minute. The dependence of the time constant for fast channel inactivation (fast component) on membrane voltage was analyzed according to Eq. (1):

$$\tau = 1/(k_0 \exp(zFV/RT)) \quad (1)$$

where $k_0$ corresponds to the rate constant for the inactivation gating transition at 0 mV and $z$ corresponds to the apparent gating charge during the open to inactivation transition. $F$, $R$, and $T$ have their usual thermodynamic meanings.

The dependence of the normalized forward rate constant for channel inactivation ($k_{on}$) or binding to PSD-95 ($k_a$) on "chain" length difference ($\Delta N$) was analyzed using a random flight model characteristic of a "ball and chain" mechanism [20,21] as parameterized by Eq. (2):

$$k_{(variant)}/k_{(wt)} = (1 + \Delta N/N)^{-n} \quad (2)$$

where $k_{(variant)}$ and $k_{(wt)}$ correspond to the respective rate constants for chimeric or deletion channel variant and the appropriate wild-type $I_LC_L$ (*ShB)* or the $I_LC_S$ (*ShA)* proteins, and $N$ corresponds to "chain" length and small $n$ to the power law value. In the case of a pure "ball and chain" mechanism a value of 3/2 is expected for n.

## CRediT authorship contribution statement

**Limor Lewin:** Data curation, Formal analysis. **Valerie Nirenberg:** Data curation, Formal analysis. **Rinat Yehezkel:** Methodology. **Shany Naim:** Methodology. **Uri Abdu:** Resources.
**Irit Orr:** Methodology. **Ofer Yifrach:** Conceptualization, Formal analysis, Funding acquisition, Supervision, Writing - original draft, Writing - review & editing.

## Acknowledgments

We thank Dr. Debbie Fass from the Weizmann Institute of Science for assistance with the ultracentrifugation analysis and Dr. Hadas Hawlena from the Ben-Gurion University for advice on statistical analyses. This research was supported by the Israel Science Foundation (Grant 294/16 to O.Y.). The authors declare that they have no conflict of interest.

## Appendix A. Supplementary data

Supplementary data to this article can be found online at https://doi.org/10.1016/j.jmb.2018.12.002.

*Received 22 July 2018;*
*Received in revised form 3 December 2018;*
*Accepted 5 December 2018*
Available online 11 December 2018

***Keywords:***
"Ball and chain";
Channel clustering;
Entropic chains;
Intrinsic disorder;
PSD-95

†Equal contributions.

***Abbreviations used:***
Kv, voltage-activated potassium channels; PSD, post-synaptic density; SPR, surface plasmon resonance; CD, circular dichroism.

## References

[1] E.R. Kandel, et al., Principles of Neural Science, McGraw-Hill, Columbus, OH, 2000.
[2] B. Hille, Ion Channels of Excitable Membranes, Sinauer Associates, Sunderland, MA, 2001.
[3] E. Kim, M. Niethammer, A. Rothschild, Y.N. Jan, M. Sheng, Clustering of *Shaker*-type $K^+$ channels by interaction with a family of membrane-associated guanylate kinases, Nature 378 (1995) 85–88.
[4] F.J. Tejedor, et al., Essential role for dlg in synaptic clustering of *Shaker* $K^+$ channels in vivo, J. Neurosci. 17 (1997) 152–159.
[5] J.S. Trimmer, Subcellular localization of $K^+$ channels in mammalian brain neurons: remarkable precision in the midst of extraordinary complexity, Neuron 85 (2015) 238–256.
[6] D. Debanne, N.C. Guerineau, B.H. Gahwiler, S.M. Thompson, Action-potential propagation gated by an axonal I(A)-like $K^+$ conductance inhippocampus, Nature 389 (1997) 286–289.
[7] K.P. Giese, et al., Reduced $K^+$ channel inactivation, spike broadening, and after-hyperpolarization in Kvbeta1.1-deficient mice with impaired learning, Learn. Mem. 5 (1998) 257–273.
[8] D. Johnston, D.A. Hoffman, C.M. Colbert, J.C. Magee, Regulation of back-propagating action potentials in hippocampal neurons, Curr. Opin. Neurobiol. 9 (1999) 288–292.
[9] P. Århem, G. Klement, C. Blomberg, Channel density regulation of firing patterns in a cortical neuron model, Biophys. J. 90 (2006) 4392–4404.

[10] H. Zeberg, C. Blomberg, P. Århem, Ion channel density regulates switches between regular and fast spiking in soma but not in axons, PLoS Comput. Biol. 6 (2010), e1000753.
[11] F.J. Sigworth, Voltage gating of ion channels, Q. Rev. Biophys. 27 (1994) 1–40.
[12] N.E. Schoppa, F.J. Sigworth, Activation of Shaker potassium channels. III. An activation gating model for wild-type and V2 mutant channels, J. Gen. Physiol. 111 (1998) 313–342.
[13] W.N. Zagotta, T. Hoshi, R.W. Aldrich, Shaker potassium channel gating. III. Evaluation of kinetic models for activation, J. Gen. Physiol. 103 (1994) 321–362.
[14] T. Hoshi, W.N. Zagotta, R.W. Aldrich, Biophysical and molecular mechanisms of *Shaker* potassium channel inactivation, Science 250 (1990) 533–538.
[15] W.N. Zagotta, T. Hoshi, R.W. Aldrich, Restoration of inactivation in mutants of *Shaker* potassium channels by a peptide derived from ShB, Science 250 (1990) 568–571.
[16] M. Zhou, J.H. Morais-Cabral, S. Mann, R. MacKinnon, Potassium channel receptor site for the inactivation gate and quaternary amine inhibitors, Nature 411 (2001) 657–661.
[17] R.W. Aldrich, Fifty years of inactivation, Nature 411 (2001) 643–644.
[18] E. Magidovich, S.J. Fleishman, O. Yifrach, Intrinsically disordered C-terminal segments of voltage-activated potassium channels: a possible fishing rod-like mechanism for channel binding to scaffold proteins, Bioinformatics 22 (2006) 1546–1550.
[19] E. Magidovich, I. Orr, D. Fass, U. Abdu, O. Yifrach, Intrinsic disorder in the C-terminal domain of the *Shaker* voltage-activated $K^+$ channel modulates its interaction with scaffold proteins, Proc. Natl. Acad. Sci. U. S. A. 104 (2007) 13022–13027.
[20] N. Zandany, S. Marciano, E. Magidovich, T. Frimerman, R. Yehezkel, T. Shem-Ad, L. Lewin, U. Abdu, I. Orr, O. Yifrach, Alternative splicing modulates Kv channel clustering through a molecular ball and chain mechanism, Nat. Commun. 6 (2015) 6488–6500.
[21] L.C. Timpe, L. Peller, A random flight chain model for the tether of the *Shaker* $K^+$ channel inactivation domain, Biophys. J. 69 (1995) 2415–2418.
[22] A.K. Dunker, et al., Intrinsically disordered proteins, J. Mol. Graph. Model. 19 (2001) 26–59.
[23] A.K. Dunker, C.J. Brown, J.D. Lawson, L.M. Iakoucheva, Z. Obradovic, Intrinsic disorder and protein function, Biochemistry 41 (2002) 6573–6583.
[24] N. Zandany, L. Lewin, V. Nirenberg, I. Orr, O. Yifrach, Entropic clocks in the service of electrical signaling: "ball and chain" mechanisms for ion channel inactivation and clustering, FEBS Lett. 589 (2015) 2441–2447.
[25] N. Zandany, O. Yifrach, A mechanistic framework for studying Kv channel clustering, Channels 9 (2015) 163–165.
[26] T.L. Schwarz, B.L. Tempel, D.M. Papazian, Y.N. Jan, L.Y. Jan, Multiple potassium-channel components are produced by alternative splicing at the *Shaker* locus in *Drosophila*, Nature 331 (1988) 137–142.
[27] O. Pongs, et al., *Shaker* encodes a family of putative potassium channel proteins in the nervous system of *Drosophila*, EMBO J. 7 (1988) 1087–1096.
[28] V.N. Uversky, Intrinsic disorder here, there, and everywhere, and nowhere to escape from it, Cell. Mol. Life Sci. 74 (2017) 3065–3067.
[29] J. Prilusky, et al., FoldIndex(C): a simple tool to predict whether a given protein sequence is intrinsically unfolded, Bioinformatics 21 (2005) 3435–3438.
[30] G. Haran, H.X. Zhou, G. Schreiber, Fundamental aspects of protein–protein association kinetics, Chem. Rev. 109 (2009) 839–860.
[31] L.C. Timpe, Y.N. Jan, L.Y. Jan, Four cDNA clones from the *Shaker* locus of *Drosophila* induce kinetically distinct A-type potassium currents in *Xenopus* oocytes, Neuron 1 (1988) 659–667.
[32] L.E. Iverson, B. Rudy, The role of the divergent amino and carboxyl domains on the inactivation properties of potassium channels derived from the *Shaker* gene of *Drosophila*, J. Neurosci. 10 (1990) 2903–2916.
[33] J.R. Topinka, D.S. Bredt, N terminal palmitoylation of PSD-95 regulates association with cell membranes and interaction with $K^+$ channel Kv 1.4, Neuron 20 (1998) 125–134.
[34] J. Rettig, et al., Inactivation properties of voltage-gated $K^+$ channels altered by presence of beta-subunit, Nature 369 (1994) 289–294.
[35] V.N. Uversky, A.K. Dunker, Understanding protein non-folding, Biochem. Biophys. Acta 1804 (2010) 1231–1264.
[36] W.R. Rice, Analyzing tables of statistical tests, Evolution 43 (1989) 223–225.